Fracture Processes in Cortical Bone: Effect of Microstructure

Simin Li, Mayao Wang, Xing Gao, Elizabeth A. Zimmermann, Christoph Riedel, Bjrn Busse and Vadim V. Silberschmidt*
V.Silberschmidt@lboro.ac.uk

Abstract

Understanding of bone fracture can improve medical and surgical procedures. Therefore, investigation of the effect of bones microstructure and properties as well as loading conditions on crack initiation and propagation is of great importance. In this paper, several modelling approaches are used to study fracture of cortical bone tissue at various length scales and different types of loading. Two major problems are tackled: crack propagation under impact loading and bone cutting in surgical procedures.

In the former case, a micro-scale finite-element (FE) fracture model was suggested, accounting for bones microstructure and using X-FEM for crack-propagation analysis [1, 2]. The cortical bone tissue was modelled as four-component heterogeneous materials. The morphology of a transverse-radial cross section captured with optical microscopy was used to generate FE models; extensive experimental studies provided necessary mechanical input data [3]. The problem of bone cutting was treated within the framework of tool-bone interaction analysis [4, 5]. A two-domain approach was used, with a process zone simulated using a smooth-particle hydrodynamics method. This zone was embedded in a continuum domain with macroscopic anisotropic properties obtained in experiments. This study is supported by analysis of damage induced by interaction between the cutting tool and the bone tissue using wedge-indentation tests and considering also the anisotropic behaviour of the bone.

1 Introduction

Research into mechanical behaviour of a natural composite material - cortical bone tissue - has attracted great attention over the past few decades, not only because of its important role in structural integrity of a musculoskeletal system, but also due to the bones intrinsic hierarchical heterogeneous structure and anisotropic mechanical properties. Macroscopically, deformation mechanisms of bones differ from those of metals, polymers and composites since bones consist of a living tissue with a continuously evolving microstructure. Mechanical properties of cortical bone vary not only from bone to bone; they demonstrate a spatial viability even within the same bone related to changes of the underlying microstructure [3, 6]. Dissimilar mechanical properties measured with indentation at different anatomical positions provide

further information on its heterogeneity and anisotropic mechanical behaviour [7]. Considering the wide spectrum of material properties of cortical bone and its intricate deformation processes associated with various loading modes and orientations, a further investigation is needed to comprehend variations of material properties in relation to the local regions and underpinning microstructural constituents.

Microscopically, complex micro-architecture of the cortical bone tissue has a significant effect on its mechanical and fracture properties. Anisotropic deformation and fracture behaviours observed at macroscopic level [8] are largely attributed to preferential alignment of micro-constituents at respective length scales, such as osteons and Haversian canals at micro-scale, or collagen fibrils and mineral crystals at nano-scale. From a fracture-toughness perspective, those intricate structural hierarchy and material heterogeneity observed in cortical bone tissues can often lead to an improved fracture resistance thanks to various toughening mechanisms [8, 9].

2 Mechanical behaviour of cortical bone tissue

2.1 Variability of anisotropic mechanical behaviour in tension and compression

Uniaxial tensile and compressive tests were conducted on specimens of cortical bone to characterise its deformation behaviours at different loading conditions and orientations.

The specimens used for this study were obtained from mid-diaphysis of fresh bovine femoral bones from a local butchery shop soon after slaughter since the mechanical behaviours of bovie and human bones are close. Specimen preparation and storage procedures followed exactly the generally adopted methods [3, 6]; details can be found in [4, 6]. Dumb-bell-shape specimens (15 mm in gauge length $\times 5\text{mm} \times$ 2 mm) oriented along both the longitudinal and transverse directions of the bone were prepared and divided into four groups according to their anatomical position (cortices, or quadrants): anterior, medial, posterior and lateral for uniaxial tension tests (Fig. 1). The same categorisation was applies to cylindrical specimens (Ø5 mm $\times$ 5 mm) for uniaxial compression test.

Experiments with specimens from four different quadrants of the bone were performed on an Instron 3366 (Instron, USA) system with a 10 kN load cell under quasi-static loading conditions. Displacements were measured using an extensometer (2630 Series, Instron) and a linear variable differential transducer (LVDT) sensor (2601 Series, Instron) in the uniaxial tensile and compressive tests, respectively. The detailed experimental procedure can be found in [6].

2.1.1 Results and analysis

The obtained results (detailed in [6]) correlate well with those reported in literature [10] and indicate that mechanical responses of cortical bone diverge dramatically under different loading conditions and orientations. Transverse specimens loaded in tension appeared to be rather brittle and failed at much lower strains compared

with those for the longitudinal direction, but the difference for compression is less prominent (Fig. 2). Regardless of the loading mode, specimens loaded in the longitudinal direction always demonstrate a higher stiffness (a higher Youngs modulus) and strength (higher ultimate stress) than those in the transverse direction. Among the material properties measured for four anatomic quadrants, two orientations and two loading modes, the anterior quadrant had the highest Youngs modulus in the longitudinal direction, while the medial quadrant has the highest one in the transverse direction. The lowest values are for the lateral and posterior quadrants for the longitudinal and transverse directions, respectively. A difference between the highest and lowest values of the Youngs modulus in each orientation was more than 20%. The relations across different quadrants (Factor A) and loading modes (Factor B) were compared in terms of significance of variances using a two-way ANOVA analysis ($\alpha = 0.05$) with a Tukey HSD test. Overall, the results showed a statistical significance in factor A (between cortices), but there is no uniform significance in factor B (between loading modes). The interaction between the two factors appears to be negative, which means that loading modes do not have effective contribution to variability across the cortices and vice versa. Results of the detailed Tukey HSD tests together with pairwise comparisons between the studied factors are summarised in [6].

2.2 Fracture toughness of cortical bone tissue

Fracture toughness of cortical bone in different orientations is studied in this section to deepen our understanding of anisotropy and variability of fracture resistance of the cortical bone tissue.

Fifteen specimens cut from each cortex of fresh bovine femurs were notched to allow crack growth along three different orientations relative to the bone axis longitudinal, transverse and radial as shown in Fig. 1. After cutting, specimens were polished and then checked under microscope to insure that their surfaces were free from scratches and damage. Specimens were kept hydrated in a 0.9% physiological saline solution prior to tests. All specimens were prepared with the same dimensions, according to British Standard: BS 7448-1: 25 mm $\times$**2.72mm**$\times$ 5.43 mm (total length $\times$**width**$\times$ thickness). Also, a very fine slit of 2.7 mm was produced using a low-speed diamond blade for all specimens according to the same standard.

The fracture toughness tests were performed on an Instron 3345 single-column bench-top machine. All specimens were loaded quasi-statically up to failure with a displacement-controlled loading rate of 1 mm/min. The load was measured using a 5 kN load cell and the corresponding load-line displacement was acquired synchronously using a LVDT sensor (2601 Series, Instron, USA), see Fig. 3. The obtained load-displacement curves were then analysed according to the classification described in BS 7448-1. After tests, fracture surfaces of all the specimens were gold-coated and analysed using scanning electron microscopy (SEM).

2.2.1 Results and analysis

Critical values of fracture toughness J_C of the cortical bone tissue were calculated for three crack-growth directions: longitudinal, radial and transverse; in addition,

anisotropy ratios of the fracture-toughness values were analysed. The obtained experimental data demonstrated that all specimens exhibited signes of a non-linear fracture process; hence, the *J*-integral (Table 1) was used to quantify fracture toughness based on British Standard: BS 7448-1.

It can be noticed from these results that the fracture-toughness values for specimens cut from different cortices vary significantly. In general, cortical bone shows higher resistance to fracture when a crack grows perpendicular to the osteon direction and lower resistance for those grow parallel to osteons (i.e. radial and longitudinal directions, respectively). For a crack growing in the transverse direction, specimens from the medial quadrant had the highest critical value of *J*-integral while those from the posterior quadrant had the lowest. The Tukey HSD test ($\alpha = 0.05$) demonstrated statistically significant differences between medial to posterior ($p = 0.035$) and posterior to lateral ($p = 0.028$) cortices. On the other hand, specimens with radially extended cracks had the highest fracture toughness for the lateral quadrant and the lowest for the posterior one. The calculated critical values of *J*-integral for the radial cracks, ranging from 983 N/m to 2664 N/m, are significantly lower compared with specimens with transverse cracks. Considerable differences were found between anterior to lateral ($p = 0.027$) and posterior to lateral ($p = 0.015$) quadrants. Finally, for specimens with cracks extending along the direction parallel to osteons (longitudinal cracks), the critical *J*-integral values were comparable with those for radial cracks, and their highest value was found for the lateral quadrant whereas anterior specimens demonstrated the lowest. Statistically significant differences in this case were found between anterior to medial ($p = 0.043$) and anterior to lateral ($p = 0.02$) quadrants. Generally, comparing the data between cortices, higher levels of fracture toughness was usually found in specimens cut from the medial and lateral quadrants. The disparity between these two groups ranged from as low as 18.3% up to 171%.

Such non-uniform fracture resistance across different cortices of the bovine femur implies that the variation of microstructure has a great impact on the local fracture processes. Previous research [3, 6] showed that a change in the volume fraction of constituents at a microstructural level largely affected local material properties, such as elastic modulus, yield stress, ultimate strength, which, in turn, influenced fracture properties. Preferential alignment of microstructural constituents also has an important effect on anisotropy of fracture toughness. Higher resistance to fracture was found for cracks propagating perpendicular to osteons, while lower resistance for cracks extending parallel to osteons. The fracture anisotropy ratios (calculated as ratios of respective values of J_C) between transversely-orientated cracks and longitudinally- or radially-orientated cracks varied for different cortices, ranging from 2.13 to 4.36, with the lowest ratio found in the lateral quadrant and the highest ratio in the anterior quadrant.

Fracture surfaces were analysed for all the tests using SEM. The results obtained for different crack-extension directions and cortex positions are grouped in Fig. 4. Dissimilar characters of fracture-surface roughness were evident among the four cortex positions an indication of a variety of fracture-toughening mechanisms acting in different cortex positions. A transition of the underlying microstructure from one type to another could be the reason for these differences. As shown in Fig. 4, the

fracture surfaces from the anterior and posterior quadrants were relatively smooth compared with those for the medial and lateral quadrants. Empirical evidence suggested that the surface roughness was associated with the amount of energy required to generate the fracture surface: a lower level of fracture energy indicates a smoother fracture surface.

Additionally, a combination of microstructural changes and different crack-extension directions triggered complicated toughening mechanisms, which, in turn, were reflected in diverse fracture-toughness values and levels of surface roughness. Generally, for the longitudinal fracture specimens, with crack fronts propagating along the direction parallel to the osteons, the fracture toughening mechanism was dominated by uncracked-ligament bridging during the process of osteons splitting, rupture, interface failure and fibre delamination (see Fig. 5 L_a, L_b). Similarly, for cracks propagating in the radial direction, the toughening mechanism was still governed by uncracked-ligament bridging as a result of osteon splitting or fibre delamination. However, a slight difference in this case was the existence of interface areas or empty spaces such as cement line or Haversian canals that had a larger contribution towards crack arrest in these regions. As a result, twists and kinks of osteons were observed in the current analysis (see Fig. 5 R_a, R_b). In contrast to the previous two cases, cracks growing along the transverse direction required a larger traction force for the crack front to penetrate and cross the osteons as longitudinal strength of osteons was much higher than transverse one. Cracks were therefore more likely to be deflected due to imperfections and heterogeneity of the microstructure or cause complete pull outs of osteons (see Fig. 5 T_a). Consequently, higher values of fracture toughness were obtained and rougher crack surfaces were observed. In the elastic-plastic fracture regime, the tensional field at the back of the crack tip also promoted a multi-scale bridging effect through shear sliding between interface regions at different levels (see Fig. 5c).

3 Numerical modelling of fracture process of cortical bone under impact loading

3.1 Model configuration for Izod test

An extended finite-element method (X-FEM) was adopted to study crack propagation in human cortical bone under dynamic loading condition. This model was developed according to the Izod test configuration shown in Fig. 6 [1]. A cortical-bone specimen was modelled as a rectangular beam with a pre-notch. Its model had two sections: a microstructured area 1.278 mm in length and 0.958 mm in width was located in front of the pre-notch as an area of interest, and a surrounding area of a homogenized bone material (50 mm in length and 8 mm in width) was implemented to reduce the overall computational cost. According to the Izod test, a loading condition was set as that of a rotational impact with 5.33 rad/s immediately before the contact with the specimen. A hammer was modelled as made of carbon steel, with isotropic material properties. Its elastic modulus, Poissons ratio

and density were 210 GPa, 0.3 and 7850 kg/m^3, respectively. A master-and-slave contact interaction between the hammer and the specimen was defined during the impact process. The bottom half of the specimen was fixed completely using an encastre-type constraint. A 4-node bilinear plain-strain quadrilateral (CPE4R) element was used in this simulation. Mechanical properties of different microstructural constituents, such as osteons, interstitial area and cement line were based on the research from Li et al. [2]. The elastic modulus of cement line was 25% lower than that of the osteons following a suggestion in Budyn et al. [11].

The model employed X-FEM to simulate crack propagation in the bone specimen. This simulation technique allows a crack to initiate and propagate along an arbitrary, solution-dependent path, subject to a local material response. The local crack initiation and evolution criteria were established using a surface-based cohesive traction-separation criterion. The initial horizontal 300 m-long crack (prenotch) was embedded into the homogenized area next to the microstructured domain (Fig. 6). Crack initiation in a cortical bone is commonly described as strain-driven; hence, a fracture strain of 0.6% was chosen based on our previous study [6]. When the fracture strain was reached, damage evolution took place. The evolution criterion was defined in terms of the fracture energy based on the fracture-toughness alues obtained in the experimental part of this study (Table 2).

3.2 Results and analysis

Four models with different statistical realizations of morphologies, obtained for four types of patients, were developed using random distributions of microstructural constituents (details in [2, 12]). The results of simulations indicated that the calculated crack-propagation paths were different for the studied groups, due to variations in spatial distributions of the microstructural constituents. Crack paths for four groups demonstrated different crack-deflection characteristics (Fig. 7) [3], with the young group having a lowest extent of deflections. For the diseased and treated groups, the crack paths exhibited more kinks compared to the other two groups. Generally, crack propagation was more influenced by surrounding cement lines and tended to go through Haversian canals. It was previously indicated that the presence of cement lines might prevent a crack from destroying other Haversian systems during the fracture process [6].

Comparing the evolution of crack lengths with time for all the studied groups, the difference was not significant, with a 6.75% standard deviation, for an average crack length of 1.419 mm. Of all the groups, the young group had the lowest crack length (1.37 mm), while it took the longest time for the crack to propagate through the microstructured area. This means that the micromorphological characteristics of bone in the young group hindered crack propagation. According to the trend curves of four groups (Fig. 7), the senior group had the lowest toughness, while the young group had the highest. For the initial 0.1 ms, the four groups had similar crack growth rates, with the senior group demonstrating a higher crack-growth rate after this. Apart from the senior group, the similar trends of crack propagation were observed in other three groups prior reaching a length of 0.4 mm; then, the crack in the diseased group began to accelerate quicker than those in the young

and treated groups, confirming a considerable improvement for the treated group compared to the non-treated group. The results obtained with the developed FE models demonstrated that micromorphology of bone played a key role in influencing the crack propagation.

4 Experimental and numerical investigation of anisotropic fracture process of cortical bone due to wedge test

To further elusidate the effect of microstructure on damage initiation and evolution in cortical bone, a study employing wedge indentation was implemented.

4.1 Experimental analysis

A total number of 40 specimens (30 mm $\times 3\mathtt{mm}\times$ 3 mm) were prepared from the mid-diaphysis of bovine femur for both longitudinal and transverse directions (Fig. 9b) using a low-speed band saw and then a diamond-coated precision blade (Isomet Low-Speed Saw, Buehler) under water irrigation. The specimens were further categorised into four groups according to their anatomic quadrants (anterior, posterior, medial and lateral) in order to reduce inconsistency caused by material variability across different regions [6]. Penetration tests were performed using Instron MicroTester 5848 with a 2 kN load cell. The specimens were kept hydrated in saline solution prior to the experiments and then glued to the testing base. Four penetrations were made for each cutting direction: perpendicular to osteons (L-C and L-R planes, Fig. 9a) and along them (C-L and C-R planes) using a standard sharp cutting tool under quasi-static loading conditions (displacement rate of 1.8 mm/min). A high-speed camera (Fastcam SA-3, Photron) equipped with a micro-lens (AF Micro-Nikkor 105mm f/2.8D, Nikon, 5000-7500 fps) was employed to capture the deformation process at micro-scale.

4.2 Modelling approach

A 3D finite-element modelling approach encompassing both conventional and smoothed-particle-hydrodynamics (SPH) elements was implemented using Abaqus/Explicit. The developed FE model was configured in accordance with our experimental setup. A plane-strain condition was assumed throughout the thickness of the tested specimen, and, therefore, to improve the computational efficiency; the cortical-bone specimen was modelled with the following dimensions: (6 mm $\times 3\mathtt{mm}\times$ 0.02 mm) (length $\times\mathtt{width}\times$ thickness), with symmetric boundary conditions applied to both front and back sides in the x-y plane as shown in Fig. 9d. The bottom surface of the specimen was fully constrained, while two lateral edges were constrained in the y-z plane. Particle elements (PC3D) were implemented in the middle part of the specimen with a width of 0.4 mm in the x-y plane (Fig. 9d). The remaining two sections were modelled using continuum elements (C3D8R). Tie constrains were applied at the boundaries between continuum and particle elements. The cutting tool

was modelled as an analytical rigid body with its geometry measured using optical microscopy.

The bovine cortical-bone specimen was modelled as transversely isotropic elasto-plastic material incorporating the Hills anisotropic yield criteria and progressive degradation. The material properties used in the model were obtained mostly in the experiments performed in this study (see Table 1 & 3).

4.3 Results and analysis

Penetration of the cutting tool was implemented in different directions: perpendicular to osteons (L-C and L-R planes) and parallel to osteons (C-L and C-R planes). The obtained results indicated strong correlation between the penetration force and orientation of the microstructure, and varied considerably across different cortices. Generally, cortical bone exhibited a higher peak force when the tool penetrated perpendicular to osteons (L-C and L-R) with more energy required to cause damage; and a significantly lower peak force when the penetration direction was parallel to osteons (C-L and C-R), due to relatively low levels of stiffness and toughness. The anisotropic ratios defined as the ratios between penetrations perpendicular to osteons and parallel to them are demonstrated in Table 4. Apparently, the anisotropy ratio varied from one cortex to another in the range from 1.43 to 2.15, with the lowest ratio found in the lateral quadrant and the highest ratio in the posterior one.

Images taken from the high-speed camera also revealed distinct deformation and damage phenomena which were largely affected by the underlying microstructures and their orientation [5]. Various microstructure-related toughening mechanisms were observed for different penetration directions. Generally, for penetration along the longitudinal axis (C-L direction) and radial direction (C-R), damage was well ahead of the cutting tip and mainly caused by material separation and subsequent crack propagation along the penetration direction (Figs.10). Deformation and damage around the cutting tip happened in a rather brittle fashion which was driven predominantly by the low stiffness in the transverse direction and the less effective longitudinal fracture resistance. As a result, low penetration forces were measured. In contrast to the previous two cases, penetrating perpendicular to osteons (L-C and L-R) required much higher force and energy due to the fact that the stiffness and fracture toughness along bone's longitudinal direction are much higher than the radial and circumferential directions. Damage was therefore more likely to be formed laterally to the penetration direction. Additionally, there were two types of damage patterns observed during our experiments on penetration perpendicular to osteons: a more brittle damage pattern involving fragmentation and materials peeling off was predominantly observed at the plexiform bone region; a more diffused ductile damage pattern was associated with large deformation of the osteonal structure.

Images taken with the high-speed camera also revealed distinct deformation and damage phenomena, which were largely affected by the underlying microstructures and their orientation [5]. Various microstructure-related toughening mechanisms were observed for different penetration directions. Generally, for penetration along the longitudinal axis (C-L direction) and the radial direction (C-R), damage was well ahead of the cutting tip and mainly caused by material separation and subse-

quent crack propagation along the penetration direction (Figs. 10). Deformation and damage around the cutting tip happened in a rather brittle fashion, driven predominantly by low stiffness in the transverse direction and the less effective longitudinal fracture resistance. As a result, low penetration forces were measured. In contrast to the previous two cases, indentations perpendicular to osteons (L-C and L-R) required much higher forces and energy due to the fact that the levels of stiffness and fracture toughness along the bone's longitudinal direction are much higher than those for the radial and circumferential directions. Damage was therefore more likely to be formed laterally to the penetration direction. Additionally, there were two types of damage patterns observed during our experiments on penetration perpendicular to osteons: (i) a more brittle damage pattern involving fragmentation and materials peeling off was predominantly observed at the plexiform bone region; (ii) a more diffused ductile damage pattern was associated with large deformation of the osteonal structure.

To gain further detailed understanding on anisotropic deformation and fracture responses to penetration of cortical bone in the vicinity of the cutting tip, numerical simulations were conducted using a SPH-based FE approach. Eight models were developed for two penetration directions (perpendicular and parallel to osteons) for each of four cortices. The performed simulations clearly demonstrated that progressive damage mechanisms strongly affected the deformation process. A comparison between the simulations and the experimental data for relationships between the levels of specific force (per unit width) and displacement demonstrated that the obtained numerical results were well within the range of the experimental measurements (see details in [5]) for different cutting directions and cortices. Apparently, the relationships between the cutting force and the penetration depth were linearly correlated up to a point somewhat below the maximum cutting force, and their initial slopes for both cutting directions were similar (Fig. 11). However, the levels of maximum force and corresponding displacement for specimens cut parallel to osteons' directions (C-L or C-R) were much lower than those for other directions. This orientation-dependent load-bearing capacity was directly affected by the distinct orientation-dependent deformation and damage mechanisms observed in our experiments (Fig. 10). By incorporating these orientation-dependent material formulation and damage mechanisms, the developed models were capable to reproduce the anisotropic character of failure, with both forces and displacements predicted adequately for various cutting directions and cortices.

5 Conclusion

In this paper, the study was focused on the fracture processes in cortical bone at various length scales. To implement it, mechanical behaviour of the cortical bone tissue was characterise for elastic, post-yield and damage regimes. The results from our studies demonstrate specific features of varying anisotropic deformation and fracture behaviours of the cortical bone tissue, which also depend on the applied loading conditions. Due to a natural loading regime exerted by species' weight and muscle forces, long bones are normally exposed to combined loading conditions that are spatially non-uniform [6]. As it is well known from the literature [8], bone is

a dynamic tissue that reacts to mechanical loading by adapting its shape, internal microstructure and material properties to meet requirements of external loading environment. The differences in the values of the Youngs modulus and fracture toughness (critical J-integral) could be the outcome of bone adaptation to its natural non-uniform loading conditions.

Combining the characterised local material properties and crack initiation and evolution techniques based on fracture mechanics, the developed microstructured model of the bone tissue adequately characterizes the non-linear fracture processes in it caused by impact loading. The further implementation of the hybrid SPH/continuum FE model enables the numerical realisation of the anisotropic deformation and damage evolution in the vicinity of the tool-bone interaction zone and povides valuble insights for further development of advanced surgical devices.

Acknowledgements

The authors acknowledge the financial support from EPSRC UK (Grant no. EP/G048886/1) and from the 7^{th} European Community Framework Programme through a Marie Curie International Research Staff Exchange Scheme (IRSES) Project TAMER (Grant PIRSES-GA-2013-610547).

References

[1] A. Abdel-Wahab, A. Maligno; V.V. Silberschmidt,Dynamic properties of cortical bone tissue: Izod tests and numerical study. CMC: Computers, Mater. Continua, 2010, Vol. 19, pp. 217-238.

[2] S. Li, A. Abdel-Wahab, E. Demirci, V.V. Silberschmidt, Fracture process in cortical bone: X-FEM analysis of microstructured models, Int. J. Fracture, 2013, Vol. 184(1), pp. 43-55.

[3] A. Abdel-Wahab, K. Alam, V.V. Silberschmidt, Analysis of anisotropic viscoelastoplastic properties of cortical bone tissues. J. Mech. Behav. Biomed. Mater., 2011, Vol. 4, pp. 807-820.

[4] S. Li, A. Abdel-Wahab, V.V. Silberschmidt, Analysis of fracture processes in cortical bone tissue, Engng. Fracture Mech., 2013, Vol. 110, pp. 448-458.

[5] S. Li, A. Abdel-Wahab, E. Demirci, V.V. Silberschmidt, Penetration of cutting tool into cortical bone: Experimental and numerical investigation of anisotropic mechanical behaviour. J. Biomech., 2014, Vol. 47, pp. 1117-1126.

[6] S. Li, E. Demirci, V.V. Silberschmidt, Variability and anisotropy of mechanical behavior of cortical bone in tension and compression. J. Mech. Behav. Biomed. Mater., 2013

[7] S. Li, E. Demirci, V.V. Silberschmidt, Analysis of Deformation Characteristics of Cortical Bone Tissue, Solid State Phenom. 188, 118-123

[8] Ritchie, R.O., Kinney, J.H., Kruzic, J.J., Nalla, R.K., A fracture mechanics and mechanistic approach to the failure of cortical bone, Fatigue Fract Engng Mater Struct 28 345-371(2005)

[9] M.E. Launey, M.J. Buehler, R.O. Ritchie, On the mechanistic origins of toughness in bone, Annu. Rev. Mater. Sci. 40 25-53(2010).

[10] D.T. Reilly, A.H. Burstein, The elastic and ultimate properties of compact bone tissue, J. Biomech. 8 393-405(1975).

[11] . Budyn, & T. Hoc, European Journal of Computational Mechanics/Revue Europenne de Mcanique Numrique, 16(2), 213-236. (2007).

[12] M. Wang, X. Gao, S.Li, A. A. Abdel-Wahab, E. A. Zimmermann, C. Riedel, B. Busse, & V. V. Silberschmidt, Effect of Micromorphology of Cortical Bone Tissue on Crack Propagation under Dynamic Loading, DYMAT. (in press)

Figures:

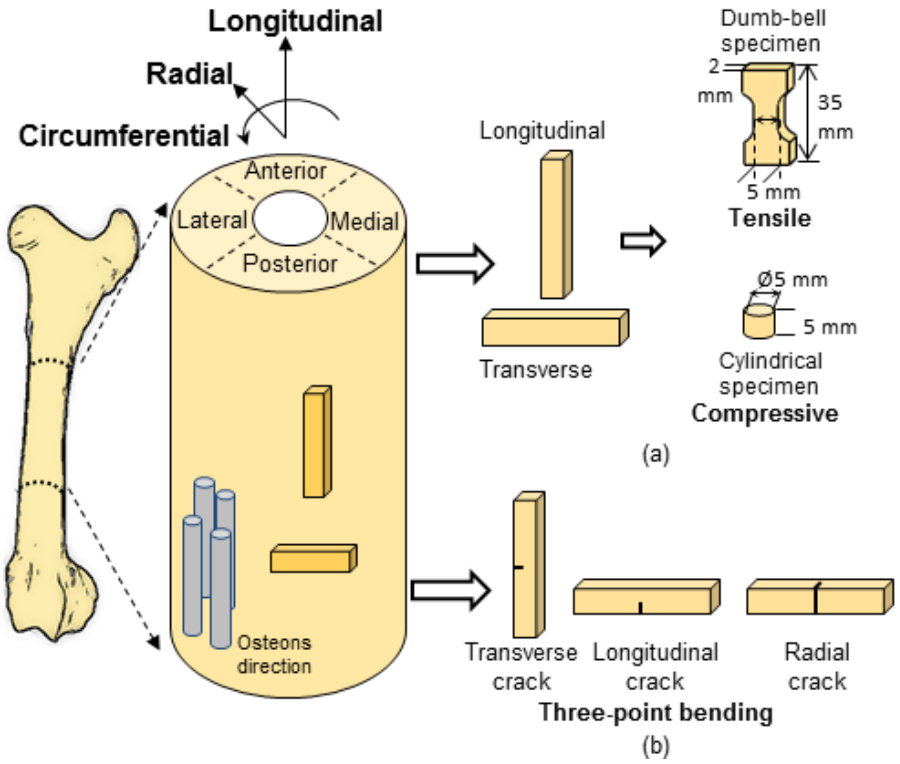

Figure 1: Fig. 1 Schematic illustration of specimen preparation process for: (a) uniaxial tension and compression tests; (b) three-point bending tests

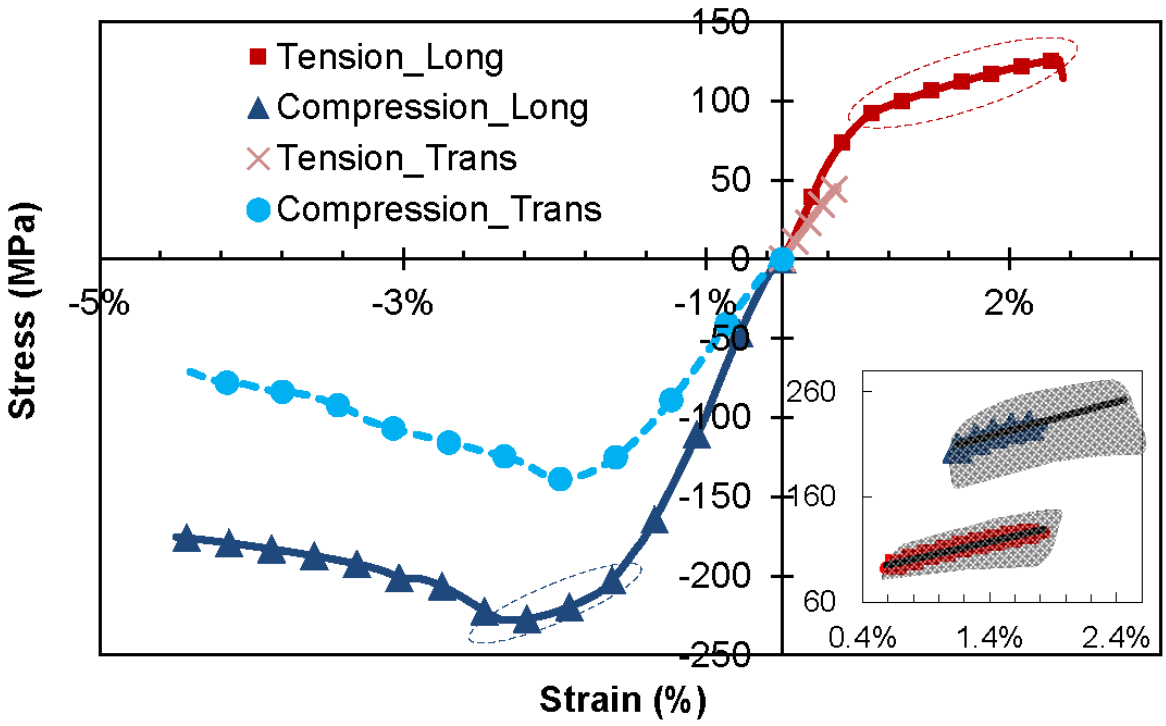

Figure 2: Fig. 2 Typical stress-strain curves for longitudinal & transverse specimens in tension and compression (anterior quadrant); Inserts show strengthening portions for longitudinal specimens

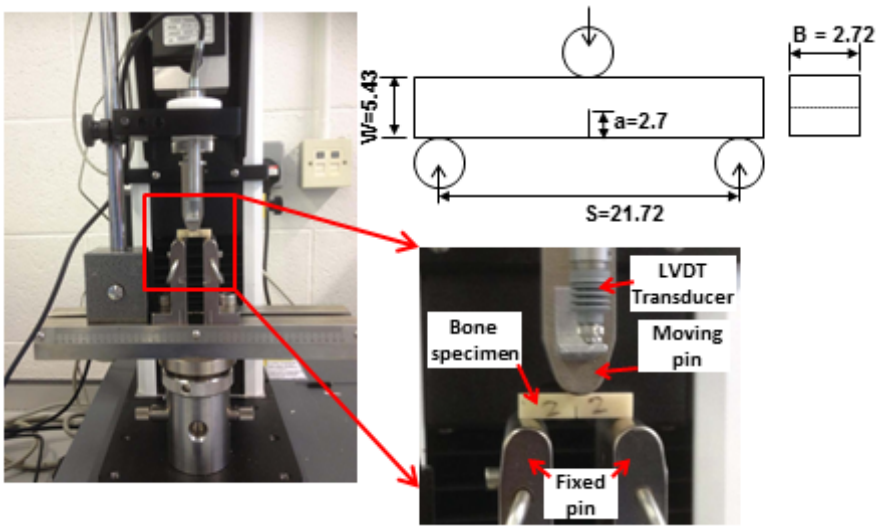

Figure 3: Fig. 3 Three-point bending test with single-edge-notch cortical bone specimen and LVDT mounted on Instron 3345

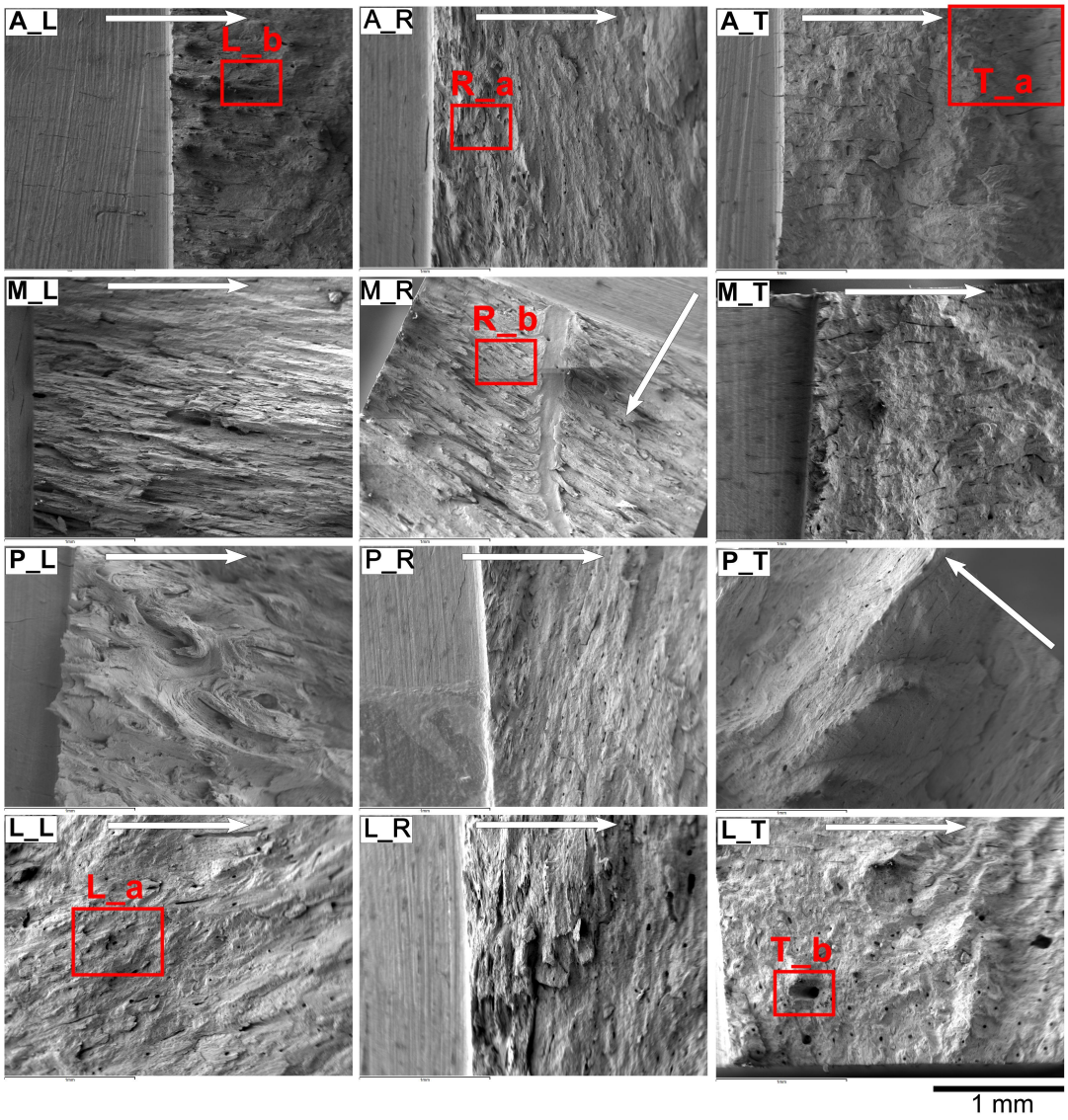

Figure 4: Fig. 4 SEM images of fracture surfaces for various cortex positions and crack propagation directions: A, M, P, L denote anterior, medial, posterior and lateral; _L, _R, _T denote crack propagation directions for longitudinal, radial and transverse ones, respectively, white arrows indicate crack growing direction

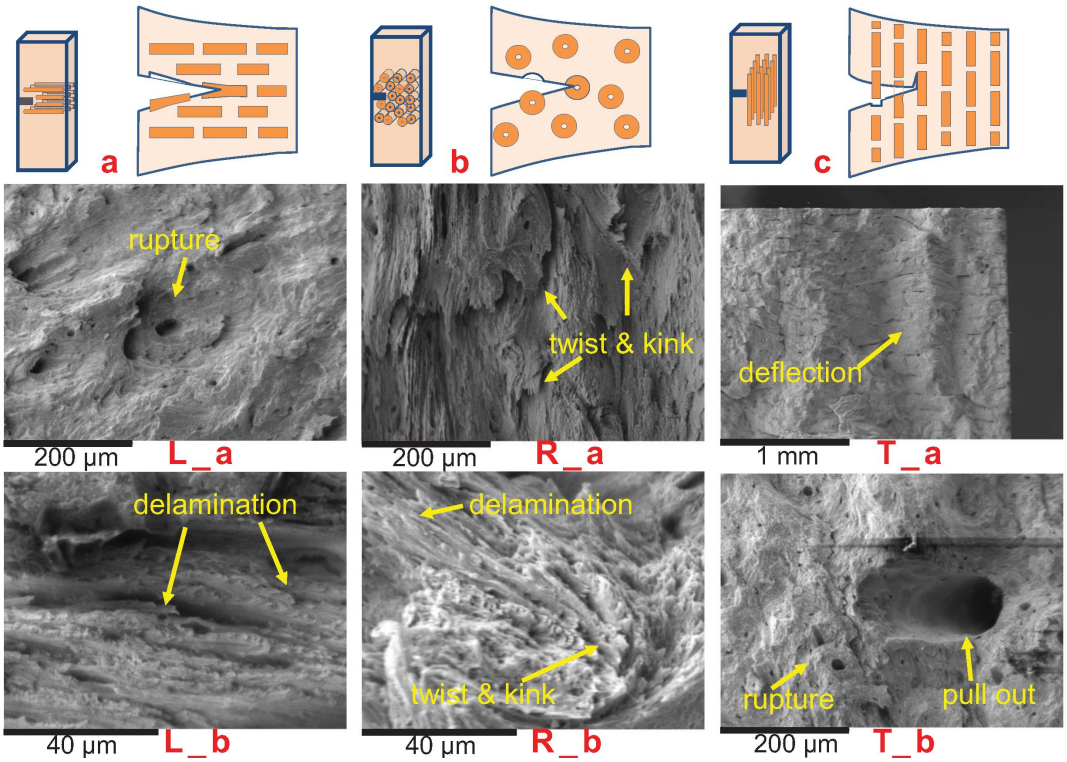

Figure 5: Fig. 5 Schematic illustrations and SEM images of various toughening mechanisms for longitudinal (a), radial (b) and transverse (c) cracks-growth directions, Labels at the bottom of each image indicate the corresponding magnified areas in Fig. 4

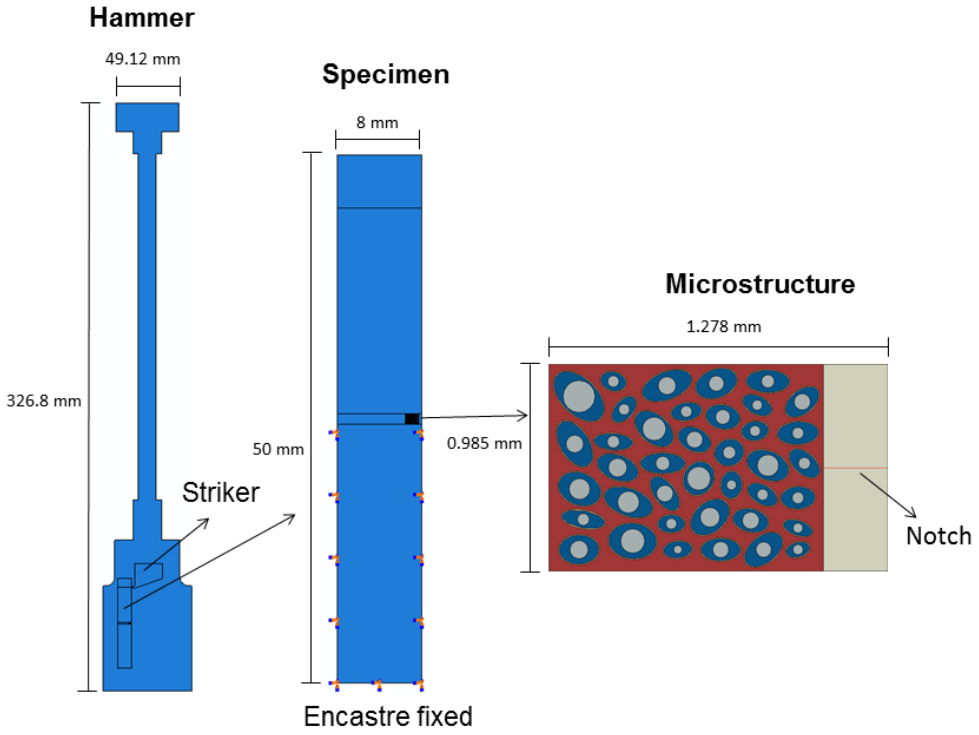

Figure 6: Fig. 6 Schematic illustrations of model configurations for Izod impact testing using microstructural bone model

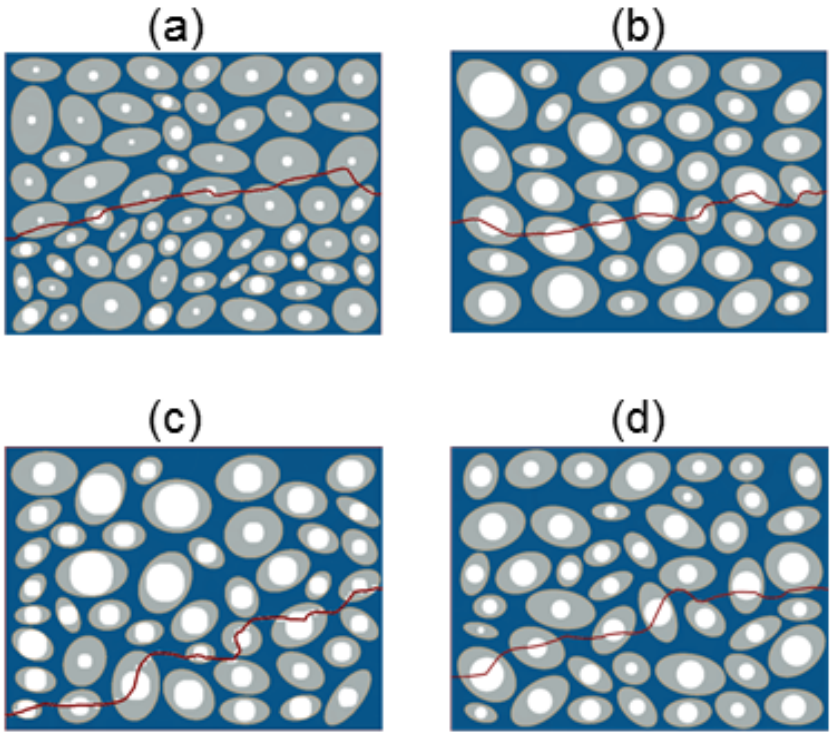

Figure 7: Fig. 7 Typical crack propagation of four different microstructure realizations (a) Young (b) Senior (c) Diseased (d) Treated

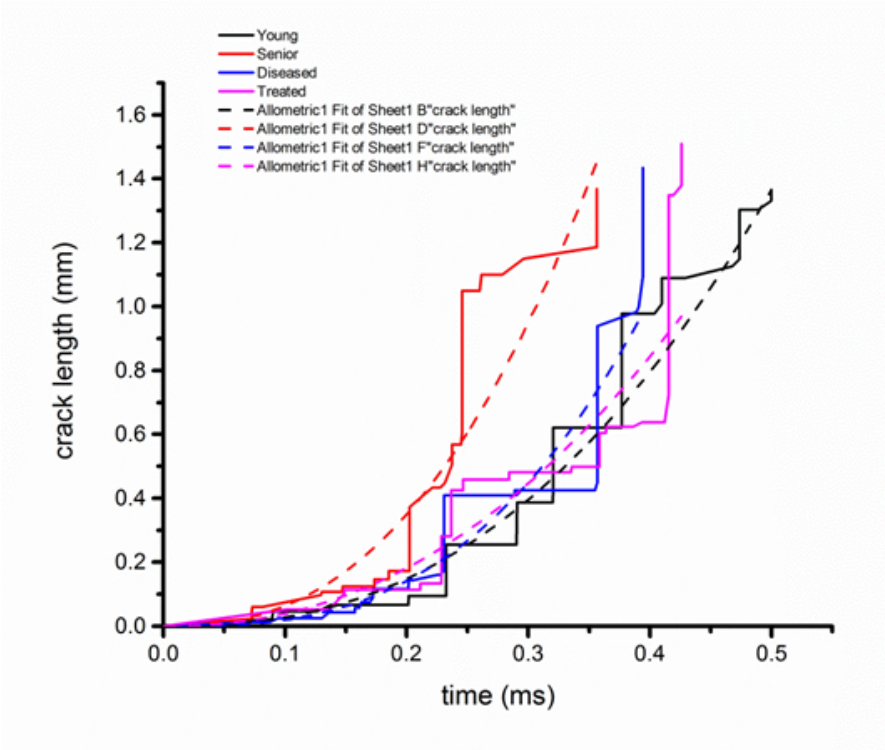

Figure 8: Fig. 8 Typical crack length versus time curves for different microstructural realizations

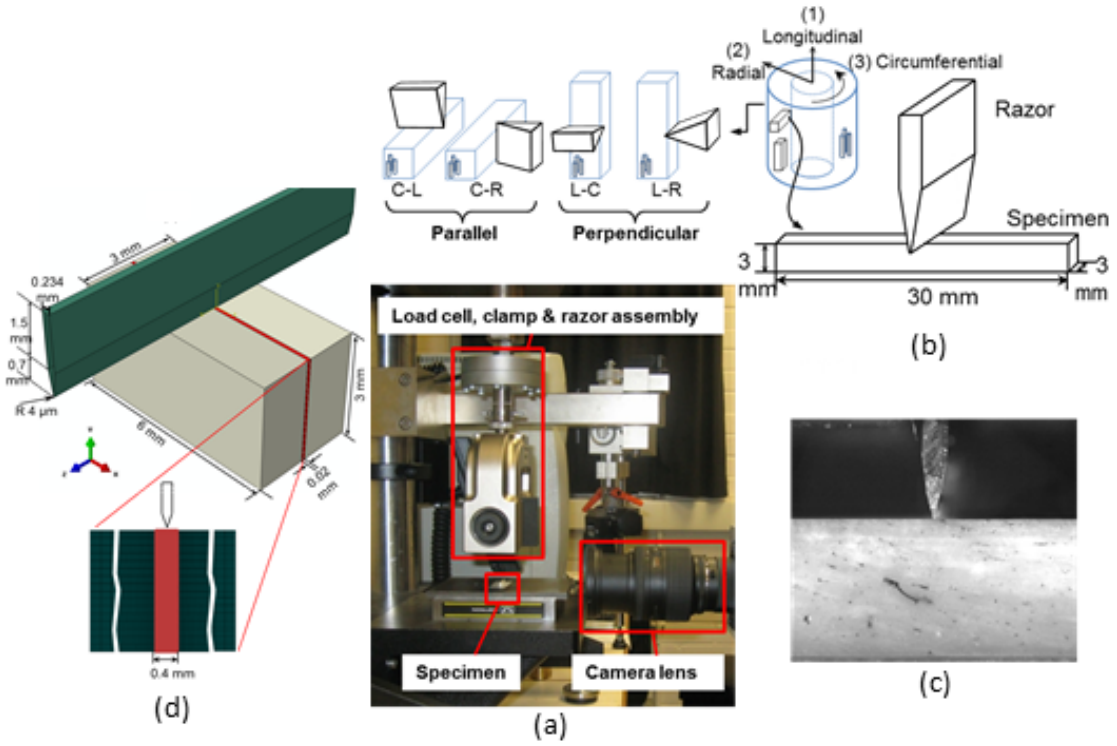

Figure 9: Fig. 9 (a) Notation of penetration directions according to ASTM E399 standard; (b) schematic of specimen preparation and cutting configuration; (c) setup for cutting experiments mounted on Instron MicroTester 5848; (c) superimposed image of razor and cortical-bone specimen taken with high-speed camera (Fastcam SA-3, Photron); (d) specification of model geometry

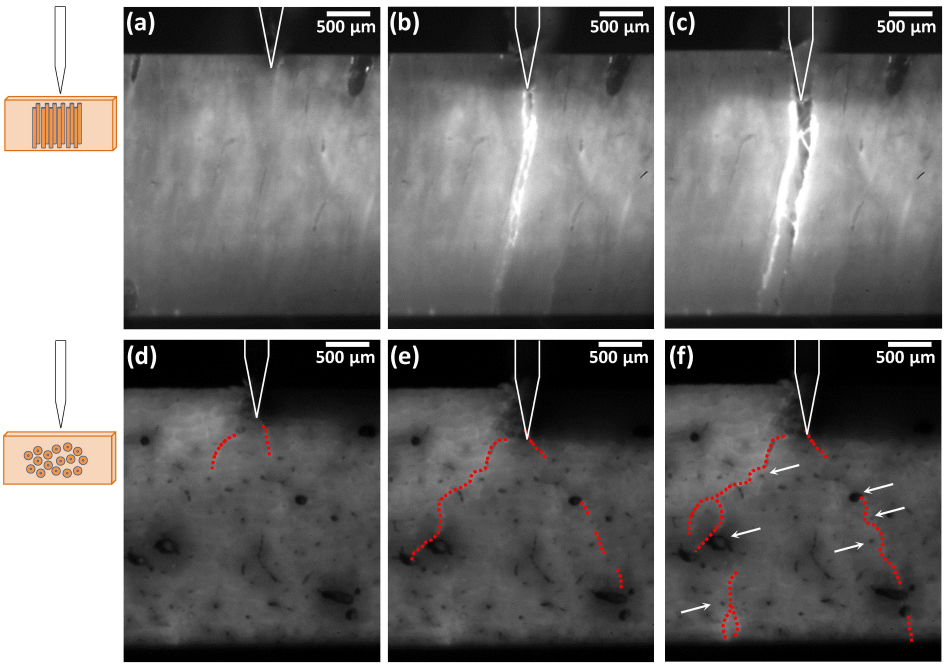

Figure 10: Fig. 10 High-speed-camera images of distinct damage processes in cutting parallel to osteons' direction,: (a-c) C-L direction; (d-f) C-R direction; white lines designate profile of razor blade, red dotted lines indicate crack path and white arrows point at positions of osteons

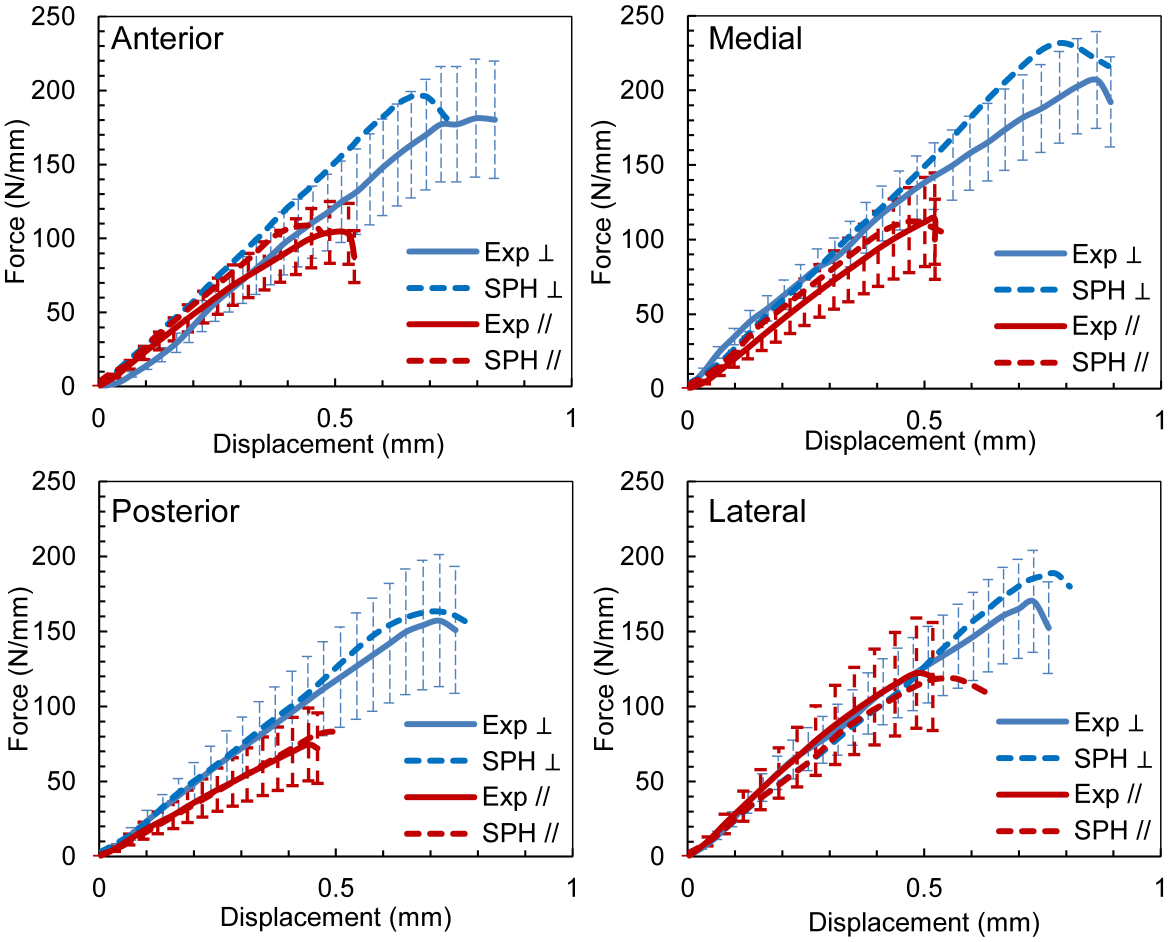

Figure 11: Fig. 11 Force (per unit width) - displacement diagrams for cutting of cortical bone in different orientations across four cortices; ⊥ and // denote penetration perpendicular and parallel to osteons' direction, respectively

Units: N/m	Anterior	Medial	Posterior	Lateral
	Mean SD	Mean SD	Mean SD	Mean SD
Longitudinal	1033.9 ±254.5	1768.5 ±98.8	1165.7 ±340.1	2034.3 ±509.9
Radial	1199.1 ±153.1	1418.2 ±97.2	983.0 ±369.5	2664.2 ±554.4
Transverse	4509.1 ±422.1	5925.5 ±802.9	3876.7 ±847.3	5661.6 ±452.7

Figure 12: Table 1 Average and standard deviation of critical J-integral values for all cortex positions and crack growth directions

	Elastic Modulus (GPa)	**Poisson's Ratio**	**Strain Energy-Release Rate (N/mm)**
Homogeneous material	10.46	0.167	0.422
Osteon	9.13	0.17	0.86
Interstitial matrix	14.122	0.153	0.238
Cement line	6.85	0.49	0.146

Figure 13: Table 2 Material properties of microstructural constituents of cortical-bone tissue and homogenous material

	Anterior	Posterior	Medial	Lateral
Density (kg/m^3)	2	2	2	2
E_1 (GPa)	23.2	19.3	21.1	15.1
E_2, E_3 (GPa)	13.2	9.9	14.7	11.2
v_{12}, v_{13}	0.27	0.27	0.27	0.27
v_{23}	0.39	0.39	0.39	0.39
G_{12}, G_{13} (GPa)	6.1	6.1	6.1	6.1
ε_{y1} (%)	1	1	1	1
ε_{f1}, ε_{f2} (%)	2	2	2	2
J_{IC1} (N/m)	1653	1534	1868	2664
J_{IC2} (N/m)	4087	3029	4765	4296

Figure 14: Table 3 Material properties used in simulations

Anisotropic ratio	Anterior	Posterior	Medial	Lateral
perpendicular /parallel	1.80	2.15	1.95	1.43

Figure 15: Table 4 Anisotropic ratios for different penetration directions for four anatomic cortices

Vadim V. Silberschmidt Wolfson School of Mechanical and Manufacturing Engineering Loughborough University Loughborough Leicestershire LE11 3TU, U.K.